Computer-Aided Civil and Infrastructure Engineering ##(200#) ##-##

Performance of vibration-based Damage Detection Methods in Bridges

Paulo J.S. Cruz[*1] and Rolando Salgado[2]

1 Associate Professor, ISISE, University of Minho, Civil Engineering Department, 4800-058 Guimarães, Portugal.

2 PhD student, ISISE, University of Minho, Civil Engineering Department, 4800-058 Guimarães, Portugal.

Abstract: The important advances achieved in the modal identification, sensors and structural monitoring of bridges have motivated the bridge engineering community to develop damage detection methods based on vibration monitoring. Some of these methods have already been demonstrated under certain conditions in bridges with deliberate damage (Farrar et al., 1998). However, the performance of these methods for damage detection in bridges has not been fully proven so far and more research needs to be done in this direction. In this article, six damage detection methods based on vibration monitoring are evaluated with two case studies. Firstly, the dynamic simulation and modal parameters of a cracked composite bridge are obtained. Here, the damage detection methods are evaluated under different crack depth, extension of the damage and noise level. Secondly, damage is identified in a reinforced concrete bridge. This bridge was deliberately damaged in two

* To whom correspondence should be addressed. E-mail: *pcruz@civil.uminho.pt*

phases. In this example, damage detection methods which do not require comparison between different structural conditions were applied. In the first case study, evaluated

damage detection methods could detect damage for all the damage scenarios; however, their performance was notably affected when noise was introduced to the vibration parameters. In the second case study, the evaluated methods could successfully localize the damage induced to the bridge.

1 INTRODUCTION

The structural performance of bridges decreases progressively throughout their service life due to many deterioration processes (fatigue, carbonation, etc). Around the world, innumerable bridges have already achieved their estimated service life and many of them have approached this limit. In the USA alone, 13.7 % (81012) of the total inventory of bridges were catalogued as structurally deficient (U.S. Department of Transportation, 2004).

The evaluation of bridge conditions has mainly been done by visual inspection. This technique depends mostly on the decisions of the bridge inspectors. Therefore, even for similar bridge conditions, a large variation in the results obtained can be expected. Furthermore, inner or too small damages can be ignored (Chase, 2001). As a result, we need more advanced techniques for damage detection in bridges.

In the last few years advanced techniques based on vibration monitoring have been proposed in order to identify damages through small changes in the dynamic response of

structures. Vibration based damage detection methods, included in this group, have lately gained more attention due to the significant advances in modal analysis methods and in monitoring technologies.

Modal Analysis methods have become a powerful tool for damage identification of bridges. The application of these methods to bridges with linear behavior has given rise to damage detection methods that use and do not use structural models. (Maeck, 2003). In former methods, the structural model of the bridge is formulated by Finite Element Methods and its modal parameters are adjusted to those obtained from the dynamic tests. Model updating methods fall in this category. In the latter methods, modal parameters obtained at different bridge damage scenarios are compared. In this article, curvature, COMAC, Damage Index, Continuous Wavelet Transform, Discrete Wavelet Analysis and Wavelet Packet Signature methods based on vibration monitoring which do not require structural model were evaluated. According to Doebling et al., (1996) these evaluated damage detection methods are classified in level 2, i.e. they can identify and localize the damage. Estimation of the damage severity and remaining service life of the structure (levels 3 and 4) are fields that need further development and they are outside of the scope of this study.

2 EVALUATED VIBRATION BASED DAMAGE DETECTION METHODS

Vibration damage detection methods are able to detect damage with information from the dynamic response of the bridge only. Several damage detection methods have been proved in different structures, materials, loads and types of damage. Methods successfully proved with certain structures, materials and kind of damage are not good in other conditions. A

general description of the most successful level 2 damage detection methods applied to the mode shapes and operating shapes of bridges will be presented.

COMAC method

One of the simplest mode shape damage detection methods is the Coordinate Modal Assurance Criterion (COMAC) method. This method measures the correlation between several vectors. If the modal displacements at node *i* of sets of mode shapes are identical, the COMAC value is one for this node. In contrast, disturbance in the damage mode shape location may give COMAC values of less than one (Ndambi et al, 2002). Its mathematical interpretation is given in Equation 1.

$$COMAC_j = \frac{\left[\sum_{i=1}^{N} \left| \{\varphi_o\}_i^j \{\varphi_D\}_i^j \right| \right]^2}{\sum_{i=1}^{N} \left[\{\varphi_o\}_i^j\right]^2 \sum_{i=1}^{N} \left[\{\varphi_D\}_i^j\right]^2}, \quad (1)$$

where $\{\varphi_o\}_i^j$ and $\{\varphi_D\}_i^j$ are the non scale mode shapes for the j^{th} node of the i^{th} mode for the baseline *o* and damaged condition *D* respectively.

Previous evaluations of this method found out that COMAC values are not low enough to clearly detect damage for all the conditions. Furthermore, false damage location can appear in undamaged zones restricting the applicability of this method. Successful detection may be obtained with this method if severe damage is present in the bridge (Salgado et al., 2006; Carrión, 2004).

Curvature method

Some time ago, it was discovered that mode shape curvature is a good parameter for damage detection. This method, proposed for the first time by Pandey et al. (1991), is based on the fact that mode shape curvature is related to the flexibility of the structure as follows

$$\kappa = \frac{d^2 y}{dx^2} = \frac{d^2 \sum_{i=1}^{\infty} \varphi_i}{dx^2} = \frac{M}{EI}, \tag{2}$$

where κ is the mode shape curvature of the cross section, M the bending moment of the cross section, E the modulus of elasticity, y is the total deflection, I the moment of inertia at that section and $d^2 \sum_{i=1}^{\infty} \varphi_i \Big/ dx^2$ the second derivative of the summation of the mode shapes with respect to the longitudinal distance, x.

In this way, if a crack appears, the flexibility of the beam (EI) will decrease causing an increment in the magnitude of the curvature.

This method has been tested on some bridges with good results (Farrar et al., 1998 and Abdel et al., 1999). The best performance of this method was obtained with severe damage and smooth mode shapes. Under these conditions, location of the damage is identified with a sharp peak. In this method, damage can be detected only with information of the damage mode shape. Better results can be obtained comparing two different structural conditions of the bridge. The main disadvantages of this method are related to the technique used for obtaining the second derivatives of the mode shapes. The central difference method is commonly used in these cases. With this technique, small regularities in the mode shapes not related to damage are also magnified, contaminating the results with several peaks.

Other methods for obtaining second derivates have been tried. However, none of them so far have solved this problem, Maeck, (2003).

Damage Index (DI) Method

This method proposed by Stubbs and Kim (1994) calculates the change in the strain energy stored in the beam when it deforms in a particular mode shape. Its formulation for discrete structural elements can be expressed as:

$$\beta_{i,j} = \frac{\{\kappa_{Di}\}_{i,j}^2 + \sum_{1}^{N} \{\kappa_{Di}\}_{i,j}^2}{\{\kappa_{oi}\}_{i,j}^2 + \sum_{1}^{N} \{\kappa_{oi}\}_{i,j}^2} \frac{\sum_{1}^{N} \{\kappa_{oi}\}_{i,j}^2}{\sum_{1}^{N} \{\kappa_{Di}\}_{i,j}^2} \tag{3}$$

where $\beta_{i,j}$ indicates the evaluation of damage at i^{th} mode at location j, N is the total number of nodes in the beam, κ is the mode shape curvature and subscripts o and D indicate the baseline and damage conditions respectively.

The DI method had an excellent performance in previous evaluations (Farrar et al., 1998 and Alvandi et al., 2006). Nevertheless, its performance depends on the accuracy of the mode shape curvatures. Therefore, it suffers from the same problems as those revealed by the curvature method.

Wavelet Analysis Methods

These methods have the ability to analyze the measured data with variable size windows making it possible to detect small singularities related to damage that other analysis methods, like Fourier Transform, cannot detect. They have been used in several fields like Structural System Identification (Adeli et al., 2006 and Jiang et al., 2007b) and

Transportation Engineering (Jiang et al., 2005). The mathematical background of these Wavelet Analysis methods applied to bridges will be briefly explained. A detailed description of the mathematical background of the wavelet analysis methods can be consulted in Mallat (1999) and Adeli et al. (2005).

Wavelet theory

Briefly, wavelets are functions that contain waves with zero mean value which drop to zero after some oscillations as represented in Equation 4.

$$\int_{-\infty}^{\infty} \Psi(x)dx = 0 \tag{4}$$

These functions with only one independent variable should satisfy the admissibility condition,

$$\int_{-\infty}^{\infty} |\Psi(x)|^2 dx < \infty \tag{5}$$

The function with these characteristics is called "mother wavelet" Ψ.

Continuous Wavelet Transform (CWT)

Different sets of mother wavelets $\Psi_{a,b}$ can be generated translating by *b* translations and dilating by *a* scales the original function. In this way, Continuous Wavelet Transform (CWT) is defined as the integral over time of the wavelet convolution. Its mathematical representation is given by,

$$CWT_{\Psi}^{f}(a,b) = \frac{1}{\sqrt{a}} \int_{-\infty}^{\infty} f(x)\Psi\left(\frac{x-b}{a}\right)dx = \int_{-\infty}^{\infty} f(x)\Psi_{a,b}dx \quad (6)$$

The results of this transformation are called wavelet coefficients and show how well the function correlates with the signal. These wavelet coefficients are very sensitive to discontinuities and singularities present in the analyzed signal. Considering this property, it was found that damage due to a sudden loss of stiffness can be detected through mode shapes with wavelet coefficients which achieve large amplitudes like a spike or an impulse in the damage location. This perturbation of wavelet coefficients due to this damage is clearer in the finest scales of the CWT. This procedure is the basis of the CWT damage detection.

Discrete Wavelet Analysis (DWA)

Discrete Wavelet Analysis (DWA), can be deduced taking advantage of the redundant information contained in CWT. In this way, it is possible to use dyadic values of dilations and translation based on powers of two without loss of accuracy. This procedure reduces the computational effort in the calculations of wavelet coefficients. For this purpose, dilation is defined as $a=2^j$ and translation parameters as $b=k2^j$ where $(j,k)\in Z$ and Z is the set of integers. In DWA, the analyzed signal is represented by approximations and details. Thus, the discrete reconstruction of the function can be expressed by

$$\begin{aligned} cD_J(k) &= \int_{-\infty}^{\infty} f(x)\Psi_{J,k}(x)dx \\ D_J(x) &= \sum_{k=-\infty}^{\infty} cD_J(k)\Psi_{J,k}(x) \\ A_J &= \sum_{j>J} D_j \\ f(x) &= A_J + \sum_{j\le J} D_j \end{aligned}, \tag{7}$$

where cD_J is the level J detail coefficients and $D_J(x)$ is the level J detail function; A_J is the approximation at level J. The DWA damage detection procedure consists of selecting a suitable mother wavelet for the analysis. Afterwards, first level details of the analyzed mode shape are examined looking for disturbance that can indicate damage.

Wavelet Packet Signature (WPS) method

This method proposed by Chang et al. (2005) calculates the operating energy shape of the analyzed structure. The method is based on The Wavelet Packet Transform (WPT). This transform is considered as a generalization of the discrete wavelet transform and can be defined as the linear decomposition of the evaluated function. Thus, a set of wavelet packets can be determined from the wavelet mother sets, just by adding a modulation $i \in Z$,

$$\Psi_{j,k}^{i} = 2^{j/2}\Psi^{i}\left(2^{j}t - k\right) \tag{8}$$

Ψ^{i} can be calculated from the following recursive relationships,

$$\Psi^{2i}(t) = \sqrt{2}\sum_{-\infty}^{\infty} h(k)\Psi^{i}(2t-k)$$
$$\Psi^{2i+1}(t) = \sqrt{2}\sum_{-\infty}^{\infty} g(k)\Psi^{i}(2t-k) \tag{9}$$

where *h(k)* and *g(k)* are the quadrature mirror filters associated with the scaling function and the mother wavelet function.

Any signal *f(t)* like dynamic response functions can be represented as the combination of wavelet packet component functions,

$$f(t) = \sum_{i=1}^{2^j} f_j^i(t) \tag{10}$$

where $f_j^i(t)$ is the linear combination of wavelet packet functions $\Psi_{j,k}^i$,

$$f_j^i(t) = \sum_{k=-\infty}^{\infty} c_{j,k}^i \Psi_{j,k}^i(t)$$
$$c_{j,k}^i = \int_{-\infty}^{\infty} f(t)\Psi_{j,k}^i(t)dt \tag{11}$$

In WPT the signal is decomposed in approximations (A) and details (D), these two results are themselves decomposed into another level of decomposition. Then this process is repeated until the required level of accuracy is achieved (see Figure 1). At the bottom of the WPT tree, $f_j^i(t)$ presents good resolution in frequency and bad resolution in time, while at the top of the WPT tree, a bad resolution in frequency and a good resolution in time are yielded. Afterwards, the energy of the dynamic response at measured points is obtained and normalized as follows:

$$E_j^i(n) = -\sum_t f_j^i(t)^2 \log\left(f_j^i(t)^2\right)$$
$$E_f = -\sum_t f(t)^2 \log\left(f(t)^2\right) = \sum_{i=1}^{2^j} E_j^i \qquad (12)$$
$$WPS_j^i(n) = \frac{E_j^i(n)}{\max(E_j^i)}$$

where, E_f and $E_j^i(n)$ are the energy of the original function and decomposed functions $f_j^i(t)$ at measuring point n respectively, $WPS_j^i(n)$ is the normalized WPS energy coefficients. The Shannon method was used for calculating the energy of the functions (Coifman et al., 1992).

The WPS method has been proved to be more tolerant to noise than the previous Wavelet Analysis methods. However, the procedure for calculating the WPT demands important computational effort at high levels of decomposition where energy WPS components are more sensitive to damage.

The damage detection procedure for WPS method consists of selecting a mother wavelet. Here, Daubechies no.4 mother wavelet was used. This mother wavelet has been proved to be good for damage detection purposes (Salgado et al., 2006). Later, dynamic response of the structures has to be decomposed and energy is calculated for each decomposed function. An arbitrary decomposed function for a high specific level of decomposition has to be chosen. No formal method exists for selecting this function; therefore several functions have to be evaluated and compared.

These methods based on Wavelet Analysis have become popular because they do not require differentiation of the measured data and it is possible to detect damage only with

the existing damage information. CWT and DWA methods are very sensitive to noise. The singularities detected with these methods in the finest scales of CWT and the first details are prone to high frequency disturbances related to noise. In any case, these methods can detect damage for a severe damage scenario. More damage detection methods based on Wavelet Analysis can be found in Peng et al. (2004) and Jiang et al. (2007)a.

More vibration based damage detection methods applied to structures can be consulted in the literature review for those methods carried out by Sohn et al. (2003) and Montalvão et al. (2006).

3 PERFORMANCE EVALUATION OF THE PROPOSED DAMAGE DETECTION METHODS

This example aims to compare the performance of the proposed damage detection methods applied to the simulated dynamic response of a composite simply supported bridge under several damage scenarios. This example tries to represent a common case found in highway bridges. Damage was analytically simulated as open cracks in the steel I beams. Dynamic simulation of the damaged bridge structure plays an important role in the damage detection process. Open vertical cracks cause a modification of the stiffness in the neighborhood of the crack. If this fact is not taken into consideration, the adopted numerical model can lead to differences in the simulated dynamic response of the damaged structures. These differences can be interpreted as false damage detection or no damage detection at all. Here, a more sophisticated procedure for obtaining the dynamic response of damaged beam structures was applied. This method was proposed for isostatic beam structures and

solutions for more complex structures are not available yet. Therefore, a more complex structural model is not justified if the cracked zone is not adequately modeled.

3.1 Bridge characteristics

The bridge considered for the evaluation of the damage detection methods represents an example of a composite simply supported bridge of 20 m length with two steel I beams (HE800B) and concrete slab with 30 MPa of compressive strength and 215 mm of depth. This bridge was designed according to the AASHTO Bridge Code, 1994 (Salgado, 2000). The geometry of this bridge is shown in Figure 2.

3.2 Damage Scenarios

In this study, damage was simulated with open cracks located in the mid-length region of the steel I beams. This simulated damage represents cracks caused by fatigue consequence of heavy traffic. The severity of damage was considered with four crack depths (see Figure 3). An initial crack of 8 mm depth appears along the bottom flange of the steel beam trying to simulate a light damage scenario (referred to as I1). In the second case, the crack propagates to 17 mm along the bottom flange (I2). In the third case, the crack covers the entire bottom flange (I3). Finally, in the last case, the crack has propagated to the half of the total depth of the steel I beam and it represents a severe damage scenario (I4). The damage extension was also evaluated using three crack patterns. One crack in the middle length of the steel beam was simulated for the first damage pattern (D1). Two cracks appear equidistant 500 mm to the first crack in the second damage pattern (D2). Finally, a further

six cracks 500 mm equidistant appear over the steel I beams (D3). The assumed damage pattern and the adopted nomenclature are illustrated in Figure 3.

3.3 Dynamic Simulations

The bridge was modeled as one dimensional simply supported composite beam according to the Euler Bernoulli hypothesis. The beam was divided in 100 elements evenly distributed along its length. Highway traffic consisting of trucks passing over the bridge at a constant speed of 80 km/h was taken into account. The truck was simulated as triple punctual loads independent of each other. Those loads had a constant axle separation of 4 m between the first and second load and 6 m between the second and third load. The magnitude for the first load was 50 kN and the remaining two loads had a uniformly distributed magnitude of between 0 and the maximum load (P=120 kN). The distance between trucks was set to 31 m according to the minimum safety distance necessary for avoiding a crash (Salgado, 2000). The adopted truck configuration over the bridge is indicated in Figure 4.

The dynamic response for cracked beams was obtained with the procedure proposed by Salgado et al. (2005) which considers that cracks cause a local change of stiffness around the location of damage. This small perturbation is taken into account during the assemblage of the general stiffness matrix. The updated mode shapes are calculated finding the eigensolution for the undamped free vibration of a typical mode considering that the bridge mass remains constant after damage. The first five mode shapes were calculated with this procedure for each damage scenario. The dynamic response of the bridge was obtained using the Higher Order Recursive Algorithm for solution of the modal equation proposed by Wilson (2002). This procedure uncouples the modal dynamic equations assuming that

classical damping exists in the structure and solving each modal equation approximating the external load with a polynomial with a small time increment. The dynamic response for the evaluated damaged bridge was obtained with a sampling frequency of 512 Hz during a recorded time of 10 seconds and considering the first five mode shapes with a damping ratio of 2%.

In the second part of the analysis, artificial noise was added to the dynamic response in order to simulate errors during acquisition of the data. Noise was considered as a normal distribution with a standard deviation equal to the chosen error on the maximum root mean square (RMS) of the response. The noise level introduced to the mode shapes and the acceleration response were 1.0%. An example of the dynamic response and calculated mode shapes for this case study are plotted in Figure 5. From this Figure it can be deduced that dynamic response with moving loads is variable enough to rule out higher noise levels. Related to mode shapes, it has been proved that high accuracy of these parameters can be obtained even in the case of strong noise contamination of the dynamic response (Brincker, 2000). Therefore this noise level is considered suitable for this evaluation.

3.4 Evaluation of damage detection methods

Damage was successfully identified when a clear spike, several spikes or local disturbance were detected in the damage zone. In this example, Daubechies 4 mother wavelet at detail no. 1 was used for damage detection for the DWA method. Gauss 4 mother wavelet at scale no. 2 was used for the CWT method. In the case of WPS method, accelerations were decomposed to the 4^{th} level using Daubechies 4 mother wavelet and the decomposed function $f_4^1(t)$ was chosen for the damage detection analysis. In Figures 6 and 7 an

example of the evaluation of damage detection methods at two levels of noise is shown. In Figure 6 all of them successfully identified the damage. In fact, damage in Figure 6 was detected in all the methods somewhat outside the damage zone. The simulated structural damage as happens in real cases, extends its influence in the vibration parameters beyond the damage zone. Therefore, this outcome does not affect the performance of the evaluated damage detection methods. In addition to these results, Tables 1 and 2 point out the sensitivity evaluation of the damage detection methods to severity of damage, extension of damage and noise level.

In Tables 1 and 2, *E* refers to clear detection of damage, i.e. the graph of the applied method presents a clear disturbance in the damage region as shown in Figure 6; *G* refers to clearer disturbance in the damage zone. In this case, the graph of the applied method presents several peaks outside the damage zone with smaller amplitudes than those located within the damage zone. When damage was not detected at all, i.e. any clear disturbance zone is located in the damage zone (see Figure 7), the evaluated methods were classified as no damage identification (-).

According to Table 1, curvature, DI, DWA, CWT and WPS methods could successfully identify damage location for all the cases. The exception was the COMAC method. In this method, peaks are not as clear as the other methods and the disturbance zone extends beyond the damage zone. Methods based on Wavelet Analysis (DWA, CWT and WPS) showed amplitudes of Wavelet coefficients extremely high at the end of the beam as shown in Figure 6. This boundary effect may hide damage located near the supports of the beam when these methods are applied to the vibration parameters of the beam.

If a noise level of 1.0% is introduced to the analyzed dynamic response and mode shapes, the evaluation of the methods is evidently affected in all the conditions (see Table 2 and Figure 7). The DWA and CWT could not identify damage in any case. These methods identify damage in the first details and finest scales composed by high frequencies, the same as the added noise that hides the singularities peaks. Curvature, DI, WPS could identify the damage for the most severe damage cases. Curvature and DI methods are more suitable for extended damage, i.e. their performance is better if several cracks are considered. On the other hand, WPS is more appropriate for localized damage, such as damage pattern D1 and D2. Furthermore, this method detected the damage location more precisely among the evaluated methods. COMAC method showed low sensitivity to noise if compared with the remaining methods. However, its performance was not satisfactory due to the fact that several peaks were detected outside the damage zone.

4 DAMAGE DETECTION IN ÖVIK BRIDGE

As an example of the applicability of the damage detection methods, dynamic tests were carried out on Övik Bridge that was object of a proof loading test until to failure. In this example, damage detection methods were evaluated under ambient vibration tests, using a limited number of data and considering two damage scenarios, i.e. under serviceability limit state and ultimate limit state. No baseline vibration parameters were obtained during the dynamic tests, i.e. dynamic response of the bridge before damage scenarios was not acquired. Moreover, dynamic tests were performed under two different structural conditions of the bridge. Consequently, only damage detection methods which did not require a comparison of the undamaged and damaged state of the bridge were considered.

From the described damage detection methods, Curvature, DWA, CWT and WPS satisfied this requirement.

4.1 Bridge Structure

Övik Bridge was built in 1955 in Örnsköldsvik, a city located in the north of Sweden. This bridge, which was part of an old railway line that has been already replaced by a new high-speed railway is a concrete frame structure with two spans of 12-12 m approximately. Its cross sections consisted of two lateral prestressed beams linked to the slab. The plan and cross sections of the bridge are shown in Figures 8 and 9 respectively.

4.2 Description of Damage Tests

The damage tests on Övik Bridge were part of the Sustainable Bridges Project related to experimental tests for evaluating the structural performance of railway bridges. The loading tests were carried out by Luleå University of Technology with the participation of several partners involved in this European project.

The failure test on Övik Bridge was divided into two main parts. In the first experimental part, named as first damage test, the bridge was loaded until the serviceability limit state (SLS). The test procedure consisted of locating a steel loading beam at the mid-length of one of the spans. Then, this loading beam was pulled out with tendons located in the two beam edges and anchored to the bedrock beneath the bridge. The load was applied to the tendons using two hydraulic jacks and this load was transmitted to the slab through the ballast as indicated in Figure 10. A bending shear failure was expected in the joint between the slab and the longitudinal beams when the tendon load achieved between 1 and 2 MN. A

visual inspection after this test showed that the damage caused by the applied force was localized in the span where the load was applied. Damage consisted of small cracks which apparently would not noticeably change the total stiffness of the bridge. An example of typical damage caused by this first load step is shown in Figure 11 (top).

In the second part of the test, named as the final failure test, the same loading procedure and the same load configuration shown in Figure 10 were adopted. However, in this case, the load was transmitted directly to the prestressed concrete beams after removing the contact supporters with the ballast. A shearing failure in the beams was expected when the tendon load achieved between 6 to 10 MN, which corresponded to the Ultimate Limit State (ULS). A visual inspection of the bridge after the final failure test confirmed that the main damage consisted of sharing failure along the point of load application. Severe damage was also present on the bottom deck of the bridge. In Figure 11 (bottom) the damage described above is shown.

4.3 Description of the Dynamic Tests

The equipment used for the dynamic tests consisted of 5 vibration sensors 941B. These sensors are able to measure displacements, velocities and accelerations with adjustable sensitivity levels. In these dynamic tests, only accelerations in vertical and longitudinal directions were recorded. These vibration sensors were connected to an amplification module which transferred the acquired information to Spider 8 Data Acquisition (DAQ) System. The vibration sensors and amplifier module used in these tests were developed by the Technical University of Beijing. The acceleration response in both dynamic tests was

acquired with a sampling frequency of 600 Hz and 300 seconds of recorded time for each setup.

Figure 12, gives a schematic representation of the 30 measuring points acquired over the bridge. To cover the total number of points with the 5 available accelerometers, 11 sensor setups were required (referred to as s-1 to s-11) with two reference sensors (referred to as r-x and r-z in longitudinal and vertical direction respectively). 22 measuring points were located on the top deck over the lateral sidewalks, measuring only vertical accelerations; the remaining 8 measuring points were located over the lateral abutments and the pillars acquiring accelerations in the longitudinal direction.

The dynamic tests on Övik Bridge were executed in two phases. The first one, referred to as the first damage test, was done on 9 July 2006, after the load achieved the SLS. During the dynamic acquisition, the loading beam and the applied load on the tendons were kept. A moderate wind with an average speed of 21 km/h in the southerly direction excited the bridge during the dynamic test. Low intensity traffic passing below one of the spans and around the bridge site was responsible for the vertical vibration of the bridge during this test.

The second dynamic test, referred to as the final failure test, was performed on 11 July 2006 after the load achieved the ULS. The loading beam and the applied load were removed before the dynamic test started. An average wind speed of 17 km/h and high intensity road traffic excited the structure during the acquisition.

In Figure 13 the acceleration histories obtained in representative locations of the bridge for both dynamic acquisition are shown. Bigger accelerations were found for the final failure

test (right column figures) compared with the first damage test (left column figures). This effect was mainly caused by the intense road traffic around the bridge.

4.4 Modal Identification after the damage tests

As mentioned before, only ambient vibration was the force excitation during the dynamic acquisition in Övik Bridge. Therefore, an Operational Modal Analysis (OMA) technique which can determine the modal parameters of the structure with just information of the dynamic response was used. In this case study, Enhanced Frequency Domain Decomposition Method (EFFD), (Brincker et al., 2001) was applied to the obtained history of accelerations for calculating the modal parameters of the bridge after the two damage tests.

The frequency range of interest after acquisition was limited to between 0 to 75 Hz. Therefore, to optimize the computational effort required during the modal analysis, the acceleration response was decimated in order 4.

In Figure 14, the Singular Value Decomposition (SVD) spectral density function of the first damage test is shown. The three largest singular value curves indicated as lines 1 to 3 were displayed. No dominant peaks associated with resonant natural frequencies were presented in this graph. Road traffic passing below the bridge responsible for the vertical excitation of this structure had a low intensity during the dynamic acquisition. Several possible frequencies were chosen along the frequency range to find feasible mode shapes. The values of the selected modal parameters and their respective standard deviations are shown in Table 3. Frequency values were determined with good confidence according to their standard deviations. On the other hand, damping ratio values showed high standard

deviations due to not well defined peaks in the spectra. The obtained mode shapes for the first damage test from the selected frequencies in the SVD spectral density function are shown in Figure 15. In this Figure, the first mode shape is mainly longitudinal with some influence of vertical bending movement. The next two mode shapes correspond to the first and second vertical bending movement. The fourth mode shape is related to vertical bending and local movement of the pillars.

In Figure 16, the SVD spectral density function for the final failure test is shown. The three largest singular value curves indicated as lines 1 to 3 were displayed. Clearer peaks than in the first damage test are present now in the probable location of resonant frequencies. The higher intensity of road traffic near the bridge during the dynamic acquisition and a more flexible structure after the final failure test highlighted the resonant frequencies in the SVD spectral density function. The resonant frequencies, damping ratios and their corresponding standard deviation are shown in Table 4. As well as in the first damage test, frequencies were calculated with good accuracy while damping ratio values were determined with high variability. Peaks associated with resonant frequencies were not enough clear for given good estimation of damping ratios. The mode shapes for the final failure test are shown in Figure 17. The first mode shape is longitudinal and same as obtained for the first damage test. Mode shapes 2 and 3 are vertical as similar in the previous modal identification. Fourth and fifth mode shapes were vertical bending movement. These two last modes may have been caused by the severe damage caused to the bridge and for the different structural configuration of the bridge during the final failure test as compared with the structural conditions of the first damage test.

In Figures 15 and 17, some mode shapes have a discontinuity in the mid-length of the left span. This discontinuity in the mode shapes cannot be taken as a final conclusion for successful damage detection, because the disturbances are not present in all the mode shapes and, they are sometimes too small to be correctly identified. Moreover, no severe damage was detected after the first damage test. Loading beam attached in their ends to stressed tendons anchored underneath the bridge during the dynamic acquisition after the first damage test may have been mainly responsible for this disruption.

4.5 Damage detection in Övik Bridge

The chosen damage detection methods (Curvature, DWA, CWT and WPS) were applied to the first two mode shapes and accelerations along the sidewalks of the bridge as an example of their applicability. Before applying the damage detection methods, the mode shapes were interpolated using piecewise cubic Hermit interpolation. The interpolation process smoothes the mode shapes reducing discontinuities not related to damage. Results of damage detection methods before and after interpolation were compared proving in this case that the interpolation process increases the performance of the methods. Furthermore, the performance of the evaluated methods is improved if more points are considered in the analysis. In the CWT method, a Gauss no. 4 mother wavelet was used for the calculations. Damage using the last method was identified in scale no. 2. Accelerations acquired in the two damage tests were decomposed using WPT until the 8th level of decomposition. Graphical inspection of all decomposed signals $f_j^i(t)$ pointed out that a clearer identification of damage was obtained for $f_8^{23}(t)$.

When the damage detection methods were applied to the vibration parameters a clear disturbance which consisted of peaks in the probable place of damage was obtained. Other peaks smaller in amplitude were also located in the end of the bridge (wings). This disturbance was caused by the he applied methods (curvature, DWA and CWT) and not by damage. The results of applying the damage detection methods in the first two mode shapes are shown in Figures 18, 19, 20 and 21. In these Figures, graphs to the left side refer to the north line, while right side graphs refer to the south line. Graphs in the top are for the first damage test and bottom graphs are for the final failure test. Abutment, pillars and Loading beam (L B) are indicated as vertical lines in these graphs. Number of modes and associated resonant frequency are also indicated for each graph.

In Figure 18, Curvature method was able to detect a big disturbance in every case near the loading beam. Here, results obtained for the first damage test (cases a, b, c and d) are very similar to those obtained results for the final failure test (cases e, f, g, and h). The same performance was obtained with DWA and CWT methods (see Figures 19 and 20). Curvature, DWA and CWT methods located the damage with sharp peaks. However, other peaks, smaller in amplitude, near the supports, are also present in Curvature and CWT methods outside the damage zone. Clearest peaks were obtained with WPS method as shown in Figure 21, but this peak in the south sidewalk is located relatively far from the damage zone. A possible reason for this behavior may be that the operating energy shape was obtained with very few points if compared with the remaining damage detection methods.

During the visual inspection after the first damage test, no severe damage was detected. However, it is possible that some severe inner damage had already taken place. In fact, the loading beam and axial loaded tendons were not removed during the dynamic test. This factor affected mode shapes mainly in a global way and evaluated damage had a local influence on the mode shapes. The disturbance detected with the damage detection methods was caused by damage present in the bridge.

In the final failure test, the position of damage for all the involved methods in the south sidewalk mode shape was located after the location of the loading beam. However, severe damage was located before the loading beam as shown in Figure 10 (bottom). This behavior can be deduced because only one sensor was located in the place of severe damage in the south sidewalk (left side of the loading beam). In contrast, three sensors were located in the north sidewalk where damage was identified in the correct place for all the damage detection methods.

5 SUMMARY AND CONCLUSIONS

The important advancement in vibration monitoring in the last years has encouraged the scientific community to develop methods based on vibration monitoring for detecting damage. In fact, the current structural evaluation of bridges needs more sophisticated methods in order to detect damage in the earliest steps. These damage detection methods have to handle several problems in order to be applied successfully to bridges. For instance, the dynamic response and modal parameters of the bridge after damage have small changes compared with the dynamic parameters from the previous structural condition. Furthermore, these methods are very sensitive to noise and temperature effects. These

factors may confuse and/or hide these small changes present in the vibration parameters. Thus, looking for more reliable methods for damage detection in bridges, six damage detection methods applied to bridges were compared and evaluated through the dynamic simulation of a composite bridge and the experimental dynamic tests in a concrete frame bridge.

In the dynamic simulation of a composite bridge, the performance of six damage detection methods of level 2 was compared. These methods could successfully identify the damage location when noise was not taken into account. When noise was added to the dynamic response and modal parameters, an abrupt decrement of successful damage location for all the methods was noticed. Curvature, DI and WPS showed the best behavior when noisy data information was given. When extensive damage and noisy data were evaluated, Curvature and DI methods were the best methods. WPS had the best performance for noisy data and not extensive damage. On the other hand, CWT and DWA were the most sensitive of noise.

In the second example in this article, damage identification of Övik Bridge was evaluated using four damage detection methods, namely the Curvature, DWA, CWT and WPS methods.

Comparison of modal parameters for the two damage tests showed that higher modes are different. It was caused by the severe damage induced to the bridge after the final failure test and the different structural configuration of the bridge during the dynamic tests.

Damage was successfully identified and localized for all the involved methods in the two analyzed damage scenarios. In the first damage test, no severe damage was detected by

visual inspection. However, it is possible that some internal damage had already taken place. Loading beam and axial loaded tendons had a global influence on the mode shapes; therefore, they were not responsible for the disturbance associated with damage for the first damage test.

In the particular evaluation of the techniques, Curvature, DWA and CWT methods could detect damage near where severe damage was localized. Nevertheless, other peaks were also localized near the supports in these methods outside the damage zone. With WPS method, a better damage identification was determined, i.e. only one peak was obtained without any disturbance outside the probable damage zone. However, damage location could not be identified as clearly as in the previous methods. Fewer points considered in the WPS methods in comparison with the other methods may make the difference.

In the final failure test, the position of damage for all the involved methods in the south sidewalk mode shape was located after the location of the loading beam. However, severe damage was located before the loading beam. This behavior can be deduced because only one sensor was located in the place of severe damage in the south sidewalk (left side of the loading beam). In contrast, three sensors were located in the north sidewalk where damage was identified in the correct place for all the damage detection methods.

In summary, the evaluated damage detection methods based on vibration monitoring are susceptible to noise. However, how noise affects the dynamic response of complex structures like bridges is difficult to predict. Several factors like severity of damage, stiffness of the bridge, location of damage, measuring points near the damage location among others may influence the performance of these damage detection methods.

6 ACKNOWELEDMENTS

The authors are grateful for the financial support provided by Sustainable Bridges for developing this research. Moreover, we would like to acknowledge the technical support given by Prof. Elfgren Lennart, Ola Enochsson and their staff at Luleå University of Technology during the execution of these tests. Finally, we wish to thank Lukasz Topczewski and Abraham Diaz de León for their valuable help during the acquisition of the dynamic tests.

7 REFERENCES

Abdel Wahab M. M. & De Roeck, G. (1999), Damage Detection in Bridges using Modal Curvatures: Application to a real damage scenario, *Journal of Sound and Vibration*, **226**(1), 217-235.

Adeli, H. & Jiang, X., (2006) Dynamic Fuzzy Wavelet Neural Network Model for Structural System Identification, *Journal of Structural Engineering*, ASCE, **132**(1),102-111.

Adeli, H. & Karim, A., (2005), *Wavelets in Intelligent Transportation Systems*, John Wiley and Sons, New York.

Alvandi, A. & Cremona C., (2006), Assessment of vibration-based damage identification techniques, *Journal of Sound and Vibration*, **292**, 179-202.

Brincker, R., Zhang, L. & Andersen, P. (2000), Modal Identification from Ambient Responses using Frequency Domain Decomposition, *Proceedings of the 18th International Modal Analysis Conference* (IMAC), St. Antonio, TX, USA.

Brincker, R., Ventura, C. E., & Andersen, P. (2001), Damping estimation by frequency domain decomposition, *Proceedings of the 19th International Modal Analysis Conference* (IMAC), Kissimmee, Florida.

Carrión, F. J. (2002), The Application of Time Frequency Intermediate Functions to the Analysis of Vibration Systems, *PhD dissertation,* School of Engineering, Autonomous University of Querétaro, Querétaro, México (in Spanish).

Chang, C. C. & Sun, Z. (2005), Structural Damage Localization using Spatial Wavelet Packet Signature, *Smart Structures and Systems,* **1**(1), 29-46.

Chase, S. B. (2001), Smarter bridges, why and how?, *Smart Material Bulletin, October*, 9-13.

Coifman, R.R., Wickerhauser M.V. (1992), Entropy-based algorithms for base basic selection, *IEEE Trans. On Inf. Theory*, **38**(2), 713-718.

Doebling, S. W., Farrar, C. R., Prime, M. B. & Sevitz, D.W. (1996), Damage identification and Health Monitoring of structural and mechanical systems from changes in their vibration characteristics: A Literature Review, *Los Alamos National Laboratory Report, LA-13070-MS*.

Farrar, C. R. & Jauregui, D. A. (1998), Comparative study of Damage Identification Algorithms applied to a bridge: I Experiment, *Smart Materials and Structures*, **7**, 704-719.

Jiang, X. and Adeli, H. (2005) Dynamic Wavelet Neural Network Model for Traffic Flow Forecasting, *Journal of Transportation Engineering*, ASCE, **131**(10), 771-779.

Jiang, X. & Adeli, H. (2007), Pseudospectra, MUSIC, and Dynamic Wavelet Neural Network for Damage Detection of Highrise Buildings, *International Journal for Numerical Methods in Engineering*, **71**(5), 606-629.

Jiang, X., Mahadevan, S., & Adeli, H. (2007), Bayesian Wavelet Packet Denoising for Structural System Identification, *Structural Control and Health Monitoring*, **14**(2), 333-356.

Maeck, J. (2003), Damage Assessment of Civil Engineering Structures by Vibration Monitoring, *PhD dissertation*, Catholic University of Leuven, Leuven, Belgium.

Mallat, S., (1999), *A wavelet tour of signal processing*, Academic Press, Second Edition.

Montalvão, D., Maia, N. M. M. & Ribeiro, A. M. R. (2006), A Review of Vibration-based Structural Health Monitoring with special Emphasis on Composite Materials, *The Shock and Vibration Digest*, **38**(4), 1-30.

Ndambi, J.-M., Vantomme, J. & Harri, K. (2002), Damage Assessment in reinforced concrete beams using eigenfrequencies and mode shape derivatives, *Engineering Structure*,**24**, 501–515

Pandey, A. K., Biswas, M. & Samman, M. M. (1991), Damage Detection from changes in curvature mode shapes, *Journal of Sound and Vibration*, **145**, 321–32.

Peng, Z.K. & Chu, F.L. (2004), Application of the Wavelet Transform in machine condition monitoring and fault diagnostics: a review with bibliography, Mechanical Systems and Signal Processing **18**, 199-221.

Salgado, R. (2000), Development of a procedure for obtaining load factors in Mexican bridges, *Master Dissertation*, National Autonomous University of Mexico, Mexico, D.F. (in Spanish).

Salgado, R. & Cruz, P. J. S. (2005), Detecting damage in structures using wavelet analysis, *The 5th international workshop on structural health monitoring; Proc. int. symp., Stanford, CA. USA*, 12-14 1809-1816.

Salgado, R., Cruz, P. J. S., Ramos, L. F. & Lourenço, P. B. (2006), Comparison between Damage Detection Methods applied to beam structures, *Proceedings, IABMAS'06* Porto, PT.

Sohn, H., Farrar, C. R., Hemez, F. M., Shunk, D. D., Stinemates, D. W. & Nadler, B. R. (2003), A Review of Structural Health Monitoring Literature: 1996-2001, *Los Alamos National Laboratory Report, LA-13976-MS, 2003*.

U.S. Department of Transportation, Federal Highway Administration FWA (2004), The Status of the Nation's Highways and Bridges: 2004 Conditions and Performance, *FHWA Report*.

Wilson, E. L. (2002), Three Dimensional Static and Dynamic Analysis of Structures: A physical approach with emphasis on earthquake engineering, Published by Computers and structures, Inc. Third Edition.

Table 1 - Evaluation of damage detection methods, noise not included.

	Damage pattern D1				Damage pattern D2				Damage pattern D3				Overall
Method	I1	I2	I3	I4	I1	I2	I3	I4	I1	I2	I3	I4	Classif.
COMAC	G	G	G	G	G	G	E	E	G	G	E	E	G
Curvature	E	E	E	E	E	E	E	E	E	E	E	E	E
DI	E	E	E	E	E	E	E	E	E	E	E	E	E
DWT	E	E	E	E	E	E	E	E	E	E	E	E	E
CWT	E	E	E	E	E	E	E	E	E	E	E	E	E
WPS	E	E	E	E	E	E	E	E	E	E	E	E	E

(E) Excellent and (G) Good.

Table 2 - Comparison of damage detection methods with noise level 1.0%.

	Damage pattern D1				Damage pattern D2				Damage pattern D3				Overall
Method	I1	I2	I3	I4	I1	I2	I3	I4	I1	I2	I3	I4	Classif.
COMAC	-	-	-	G	-	-	G	G	-	-	G	G	G
Curvature	-	-	-	E	-	-	G	G	-	-	-	E	G
DI	-	-	-	E	-	-	G	G	-	-	E	E	G
DWT	-	-	-	-	-	-	-	-	-	-	-	-	-
CWT	-	-	-	-	-	-	-	-	-	-	-	-	-
WPS	-	-	-	E	-	-	-	E	-	-	-	G	G

(E) Excellent, (G) Good and (-) No damage identification.

Table 3 – Frequencies and damping ratios for the first damage test

	Hz		%	
Mode	Frequency	Standard dev freq	Damping ratio	Standard dev damp
1	6.33	0.05	2.88	1.72
2	15.48	0.10	1.11	0.71
3	18.62	0.09	2.22	1.47
4	43.00	0.04	0.51	0.37

Table 4 – Frequencies and damping ratios for the final failure test

	Hz		%	
Mode	Frequency	Standard dev freq	Damping ratio	Standard dev damp
1	6.25	0.12	6.42	1.61
2	12.65	0.05	1.78	0.58
3	17.24	0.05	1.98	1.96
4	25.04	0.04	0.58	0.42
5	34.46	0.13	0.59	0.61

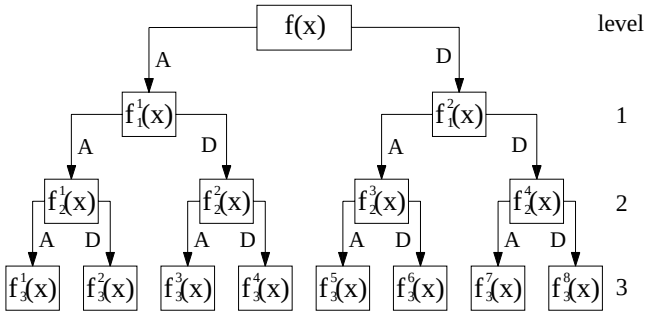

Figure 1 - Wavelet Packet Transform at 3rd level of Decomposition.

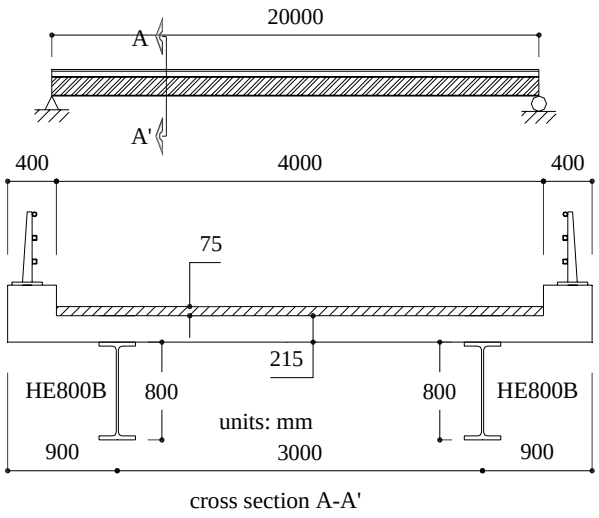

Figure 2 - Geometry of the composite bridge adopted as example.

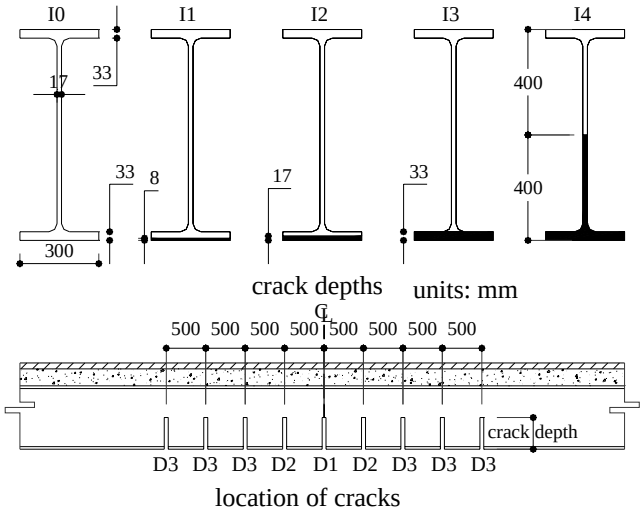

Figure 3 - Assumed damage scenarios.

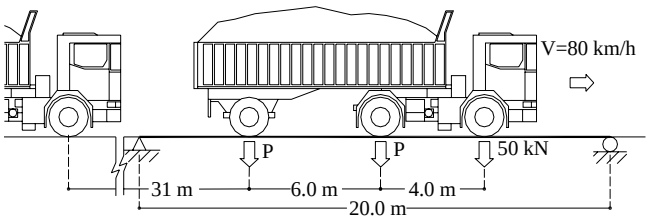

Figure 4 - Truck configuration considered for the dynamic simulations.

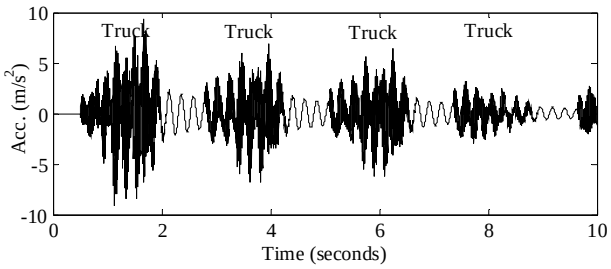

a) Acceleration history for the mid-length point.

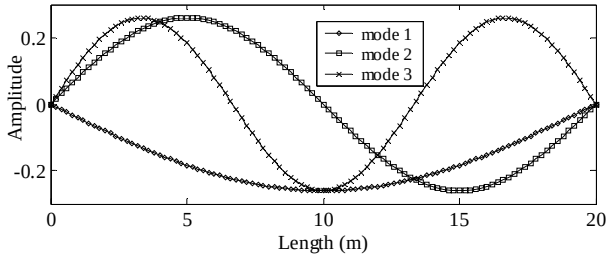

b) Three first mode shapes for the undamaged case

Figure 5 –Typical example of the acceleration history and mode shapes of the bridge.

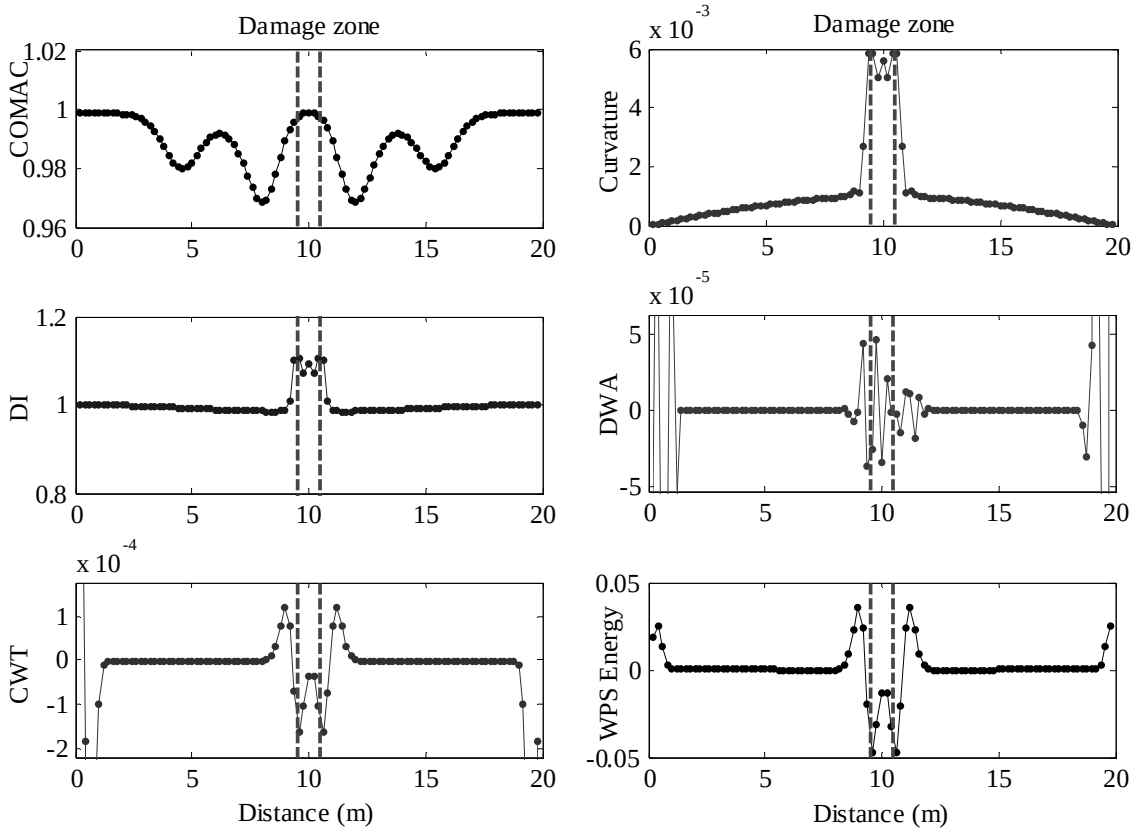

Figure 6 - Typical comparison of level 2 damage detection methods (crack depth I4 and crack location D2, noise not added).

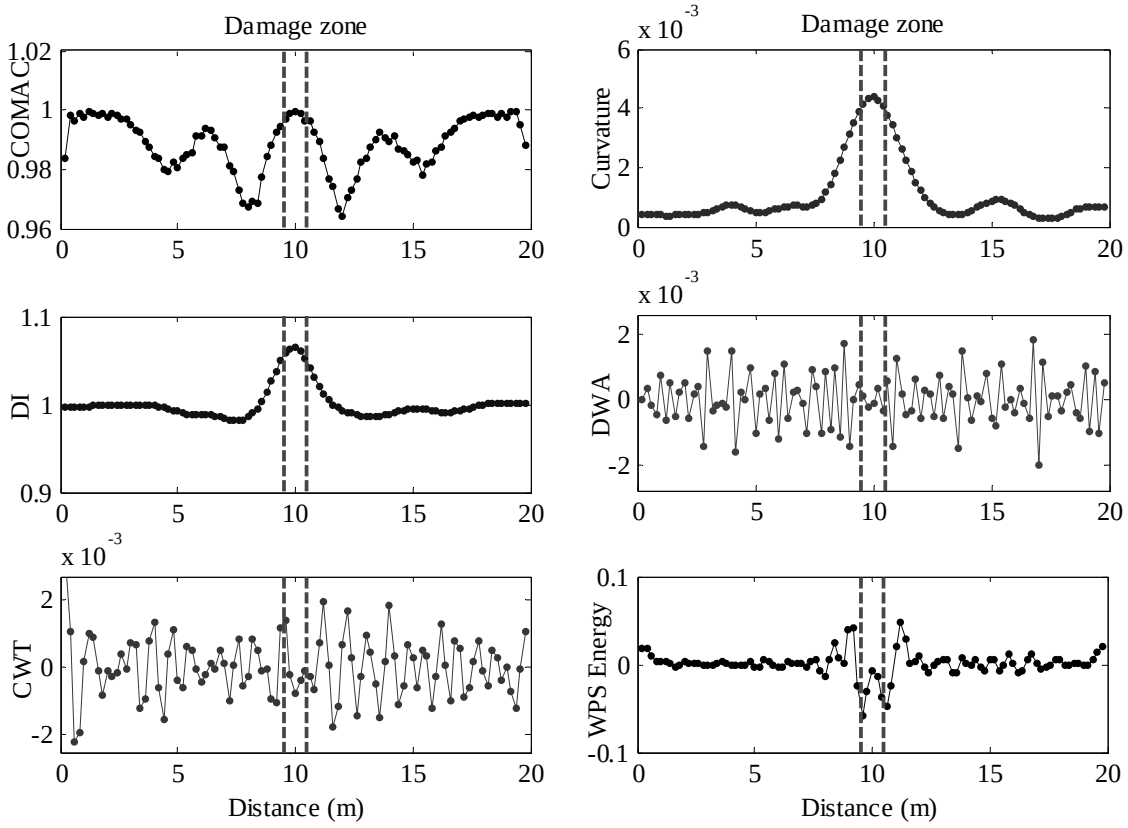

Figure 7 - Typical comparison of level 2 damage detection methods (crack depth I4 and crack location D2, noise level 1.0%).

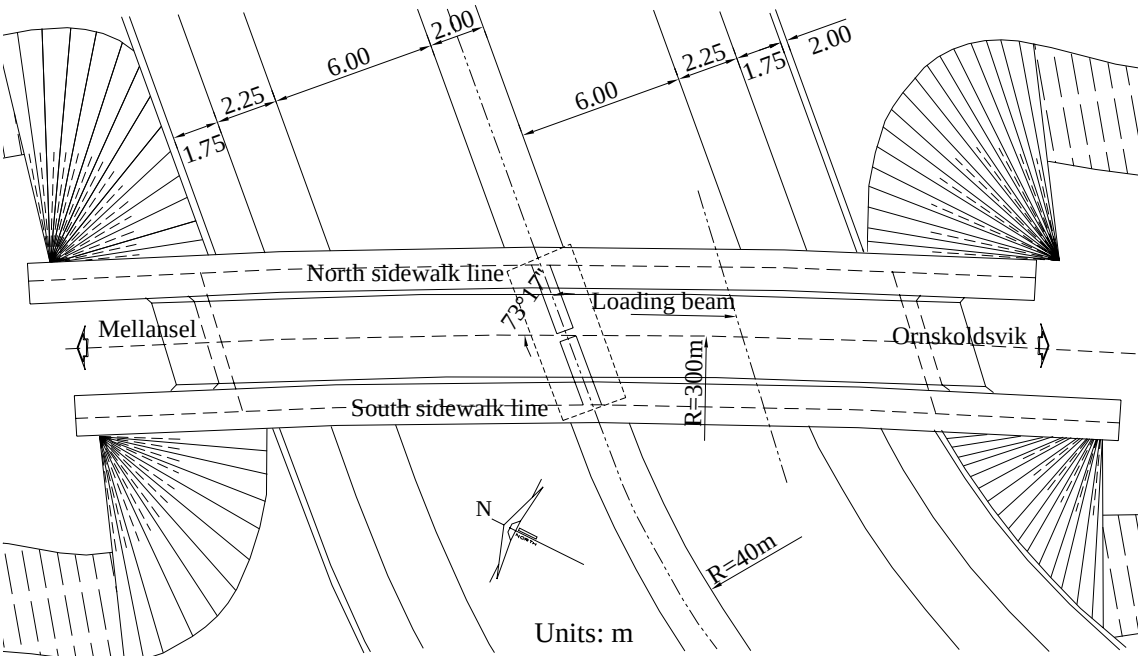

Figure 8 - Plan of Övik Bridge.

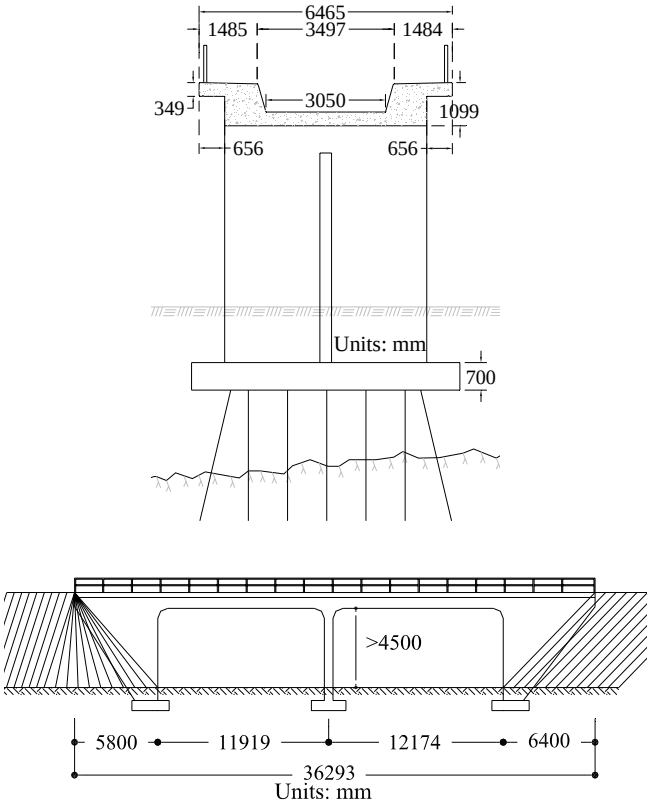

Figure 9 - Cross sections.

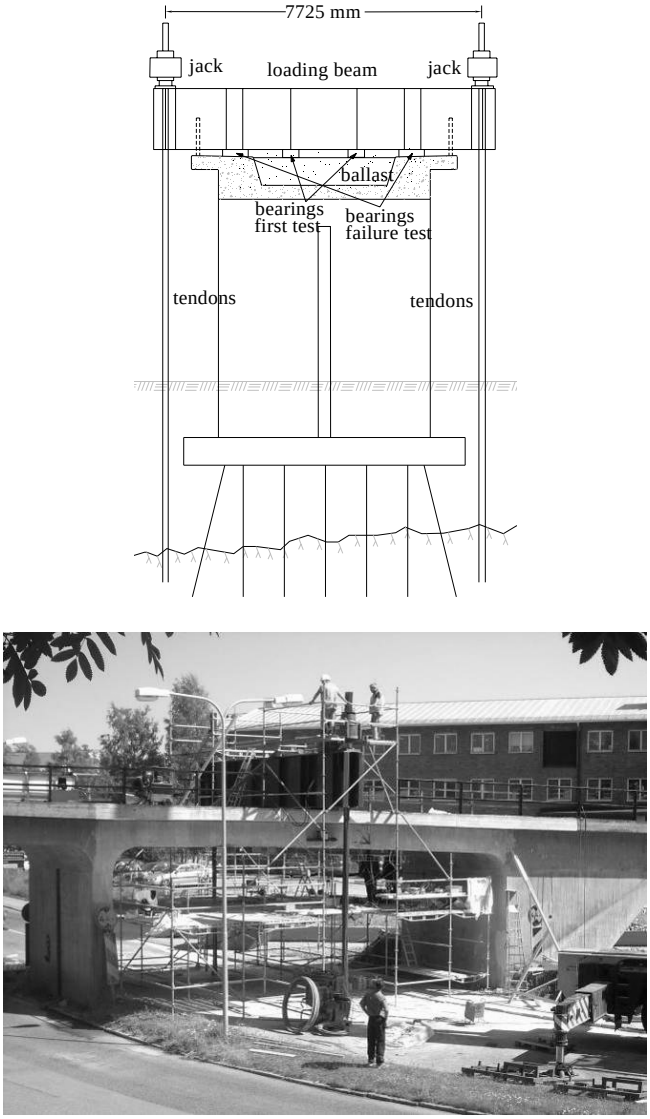

Figure 10 - Loading beam location for the damage tests.

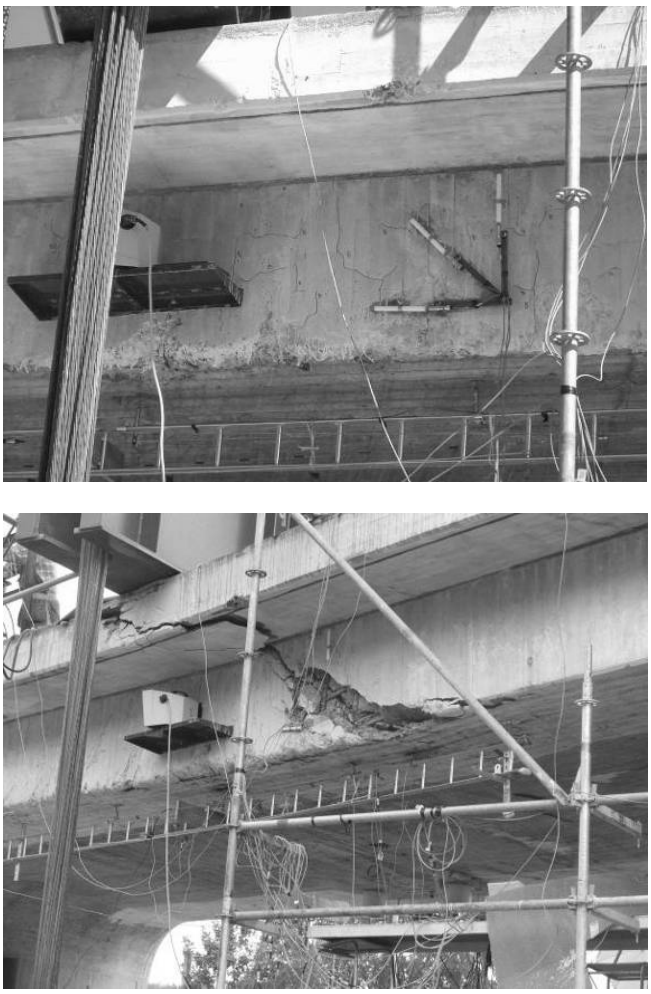

Figure 11 - Cracking in the lateral beam; (top) first damage test; (bottom) final failure test.

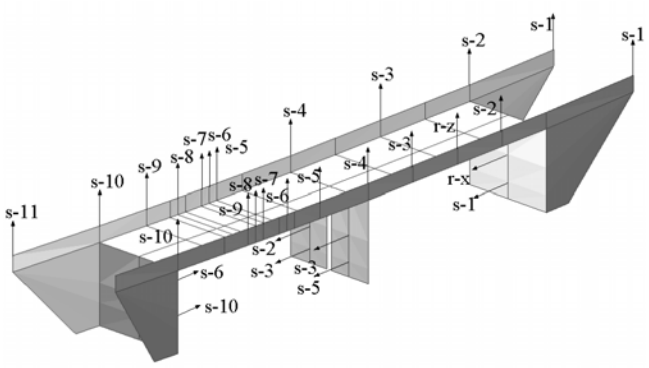

Figure 12 – Layout of measuring points for the dynamic tests in Övik Bridge.

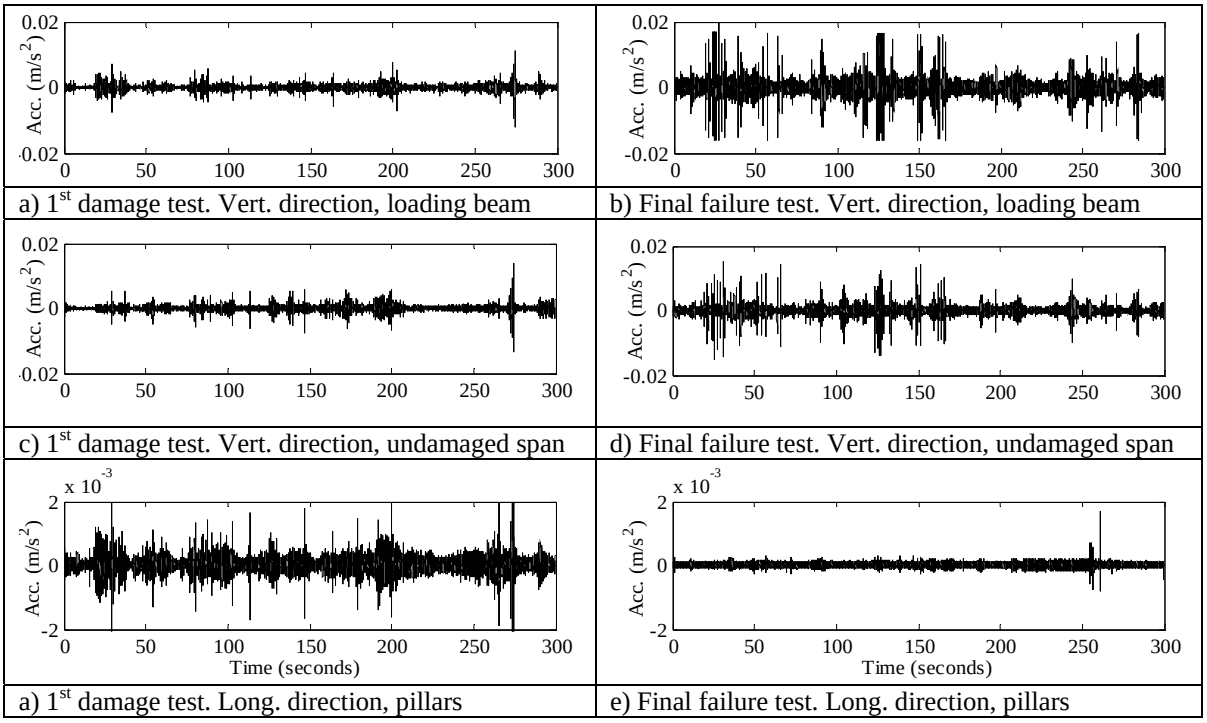

Figure 13 – Comparison of the acceleration histories in some location in the bridge.

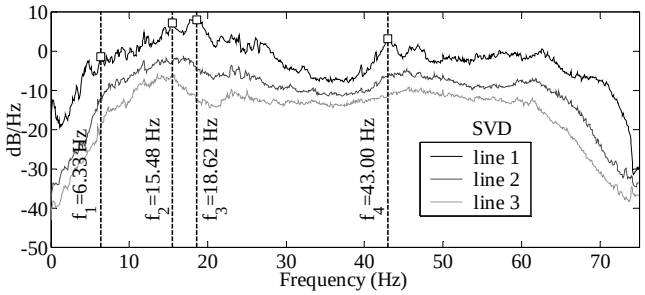

Figure 14 – Singular Values of the Spectral Density Function for all setups in the first damage test.

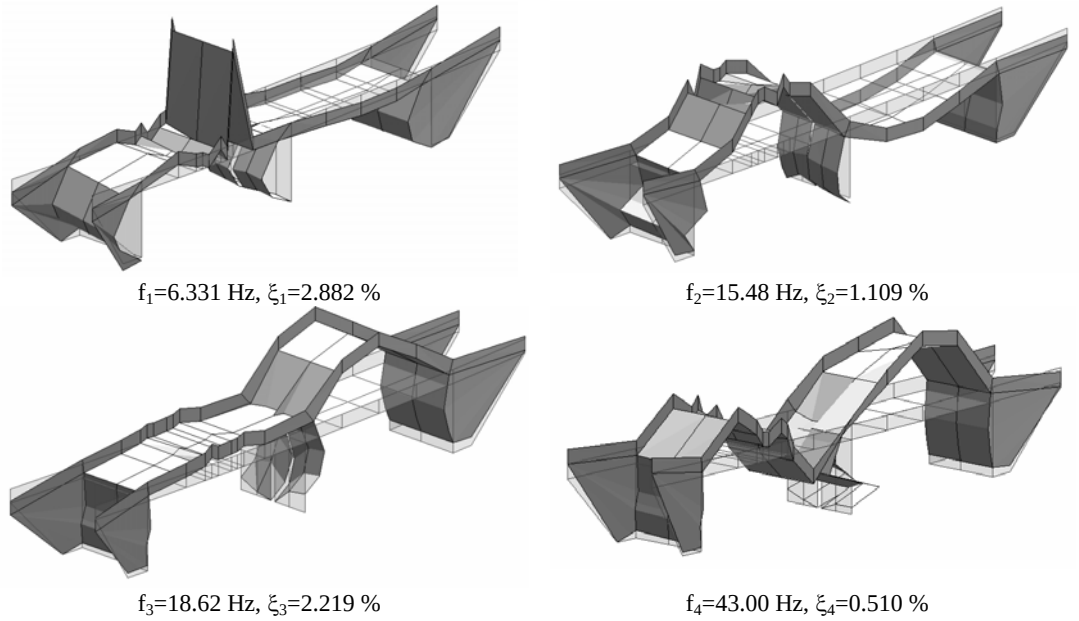

f_1=6.331 Hz, ξ_1=2.882 %

f_2=15.48 Hz, ξ_2=1.109 %

f_3=18.62 Hz, ξ_3=2.219 %

f_4=43.00 Hz, ξ_4=0.510 %

Figure 15 - Estimated mode shapes for the first damage test.

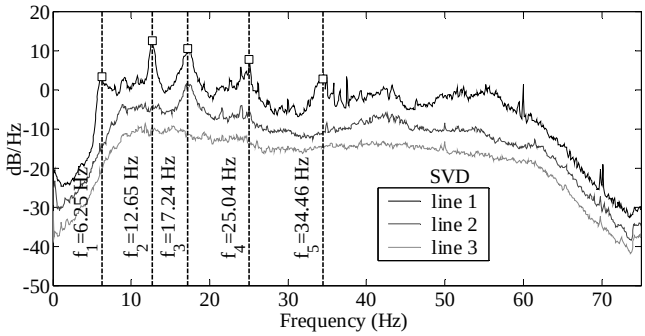

Figure 16 – Singular Values of the Spectral Density Function for all setups in the final damage test.

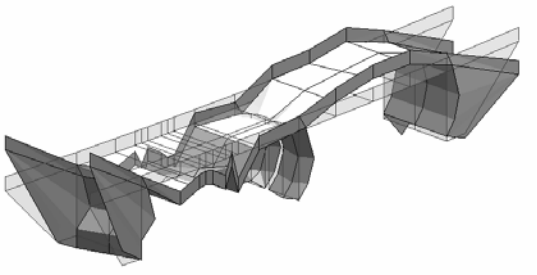

f_1=6.246 Hz, ξ_1=6.415 %

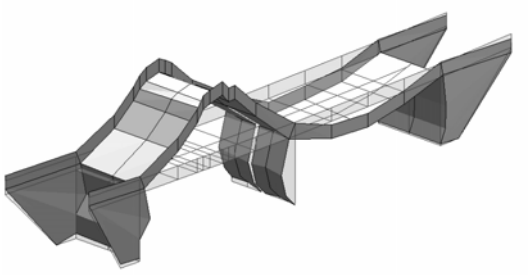

f_2=12.65 Hz, ξ_2=1.781 %

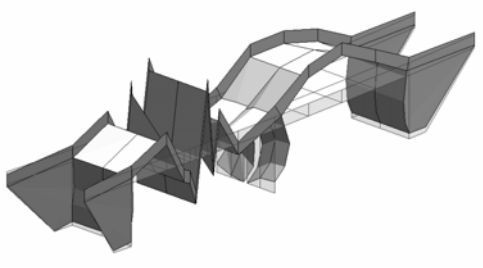

f_3=17.24 Hz, ξ_3=1.976 %

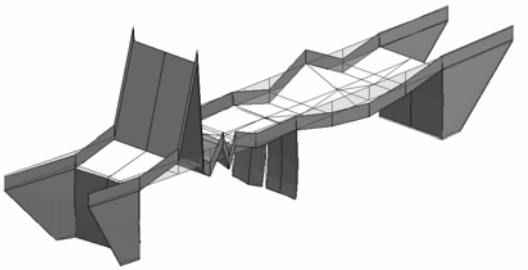

f_4=25.04 Hz, ξ_4=0.576 %

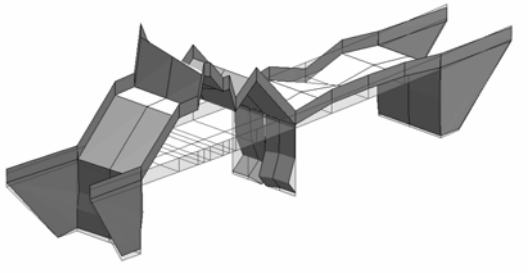

f_5=34.46 Hz, ξ_5=0.592 %

Figure 17 - Estimated modal parameters for the final failure test.

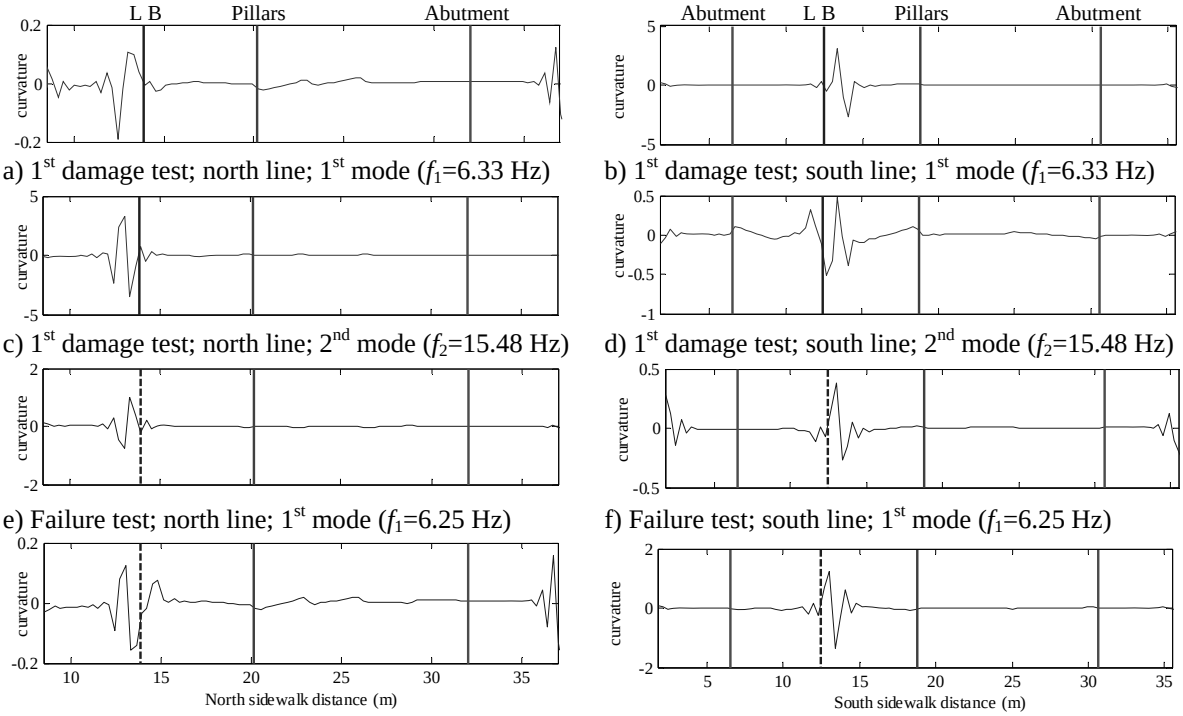

a) 1st damage test; north line; 1st mode (f_1=6.33 Hz)

b) 1st damage test; south line; 1st mode (f_1=6.33 Hz)

c) 1st damage test; north line; 2nd mode (f_2=15.48 Hz)

d) 1st damage test; south line; 2nd mode (f_2=15.48 Hz)

e) Failure test; north line; 1st mode (f_1=6.25 Hz)

f) Failure test; south line; 1st mode (f_1=6.25 Hz)

g) Failure test; north line; 2nd mode (f_2=12.65 Hz)

h) Failure test; south line; 2nd mode (f_2=12.65 Hz)

Figure 18 - Curvature method applied to the first two mode shapes in the deck of the bridge.

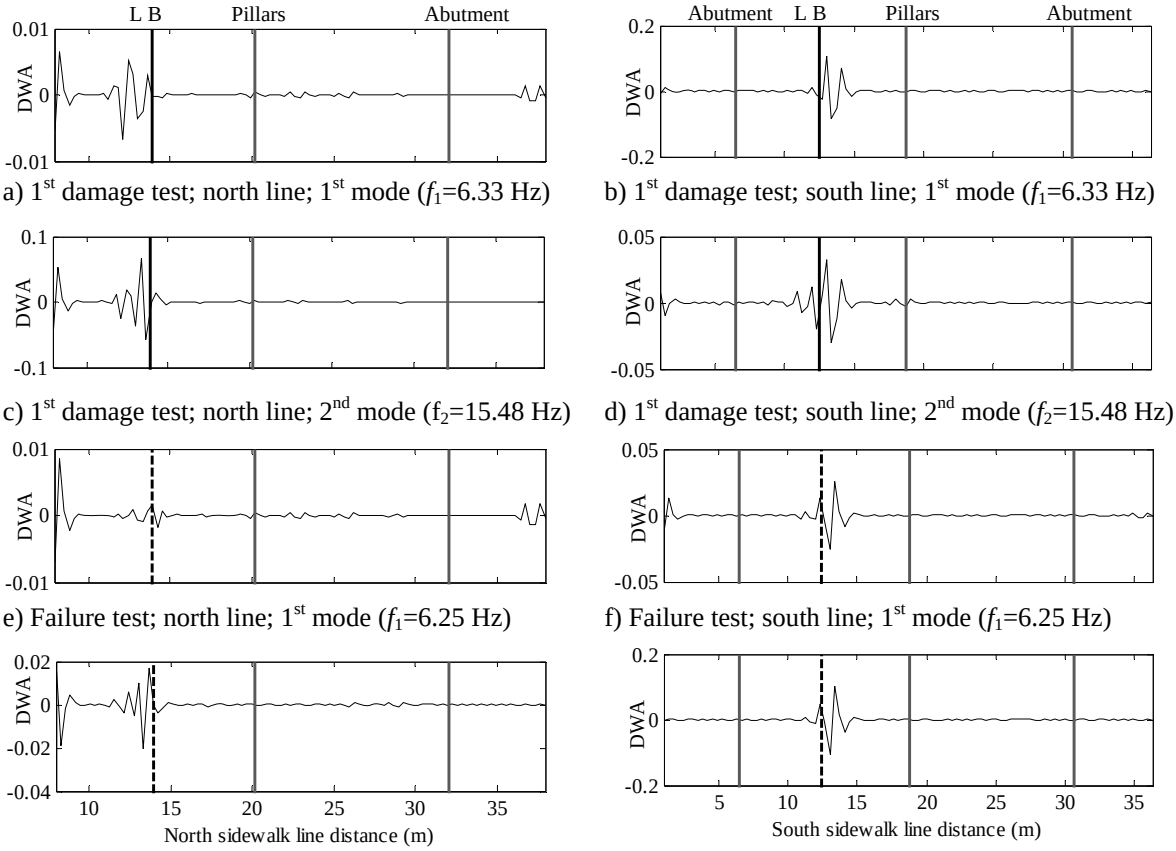

a) 1st damage test; north line; 1st mode (f_1=6.33 Hz)

b) 1st damage test; south line; 1st mode (f_1=6.33 Hz)

c) 1st damage test; north line; 2nd mode (f_2=15.48 Hz)

d) 1st damage test; south line; 2nd mode (f_2=15.48 Hz)

e) Failure test; north line; 1st mode (f_1=6.25 Hz)

f) Failure test; south line; 1st mode (f_1=6.25 Hz)

g) Failure test; north line; 2nd mode (f_2=12.65 Hz)

h) Failure test; south line; 2nd mode (f_2=12.65 Hz)

Figure 19 -DWA method applied to the first two mode shapes in the deck of the bridge.

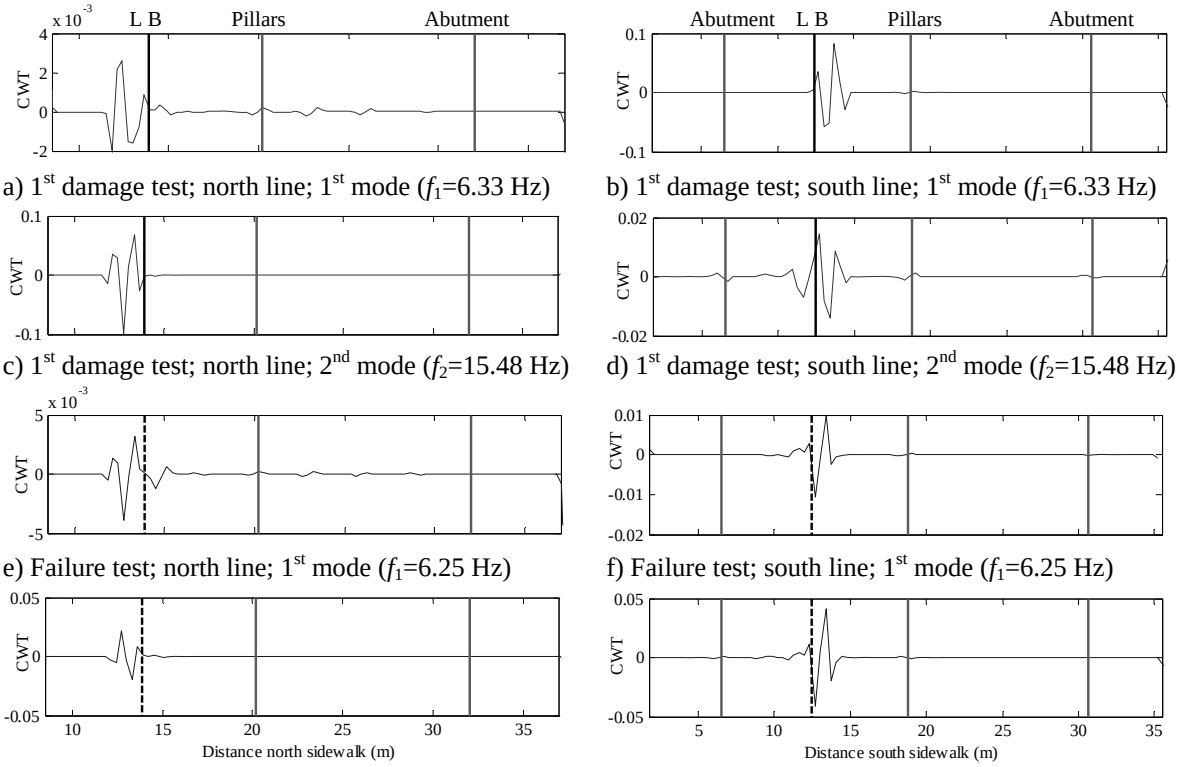

a) 1st damage test; north line; 1st mode (f_1=6.33 Hz)

b) 1st damage test; south line; 1st mode (f_1=6.33 Hz)

c) 1st damage test; north line; 2nd mode (f_2=15.48 Hz)

d) 1st damage test; south line; 2nd mode (f_2=15.48 Hz)

e) Failure test; north line; 1st mode (f_1=6.25 Hz)

f) Failure test; south line; 1st mode (f_1=6.25 Hz)

g) Failure test; north line; 2nd mode (f_2=12.65 Hz)

h) Failure test; south line; 2nd mode (f_2=12.65 Hz)

Figure 20 - CWT method applied to the first two mode shapes in the deck of the bridge.

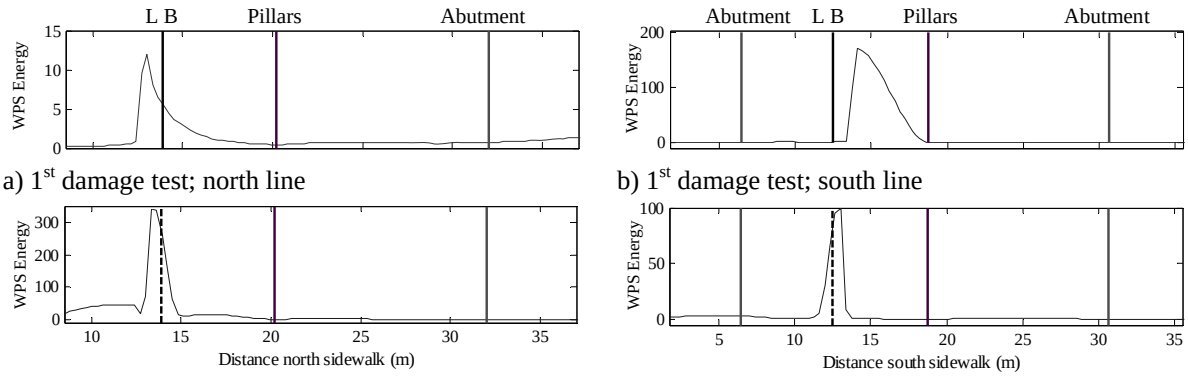

a) 1st damage test; north line

b) 1st damage test; south line

c) Failure test; north line

d) Failure test; south line

Figure 21 - WPS applied to the acceleration along the deck of the bridge.